

# Competing Exchange Interactions in the Multiferroic and Ferrimagnetic $\text{CaBaCo}_4\text{O}_7^*$

R.S. Fishman<sup>1</sup>, S. Bordács<sup>2</sup>, V. Kocsis<sup>2</sup>, I. Kézsmárki<sup>2</sup>, J. Viirik<sup>3</sup>, U. Nagel<sup>3</sup>, T.

Rõm<sup>3</sup>, A. Puri<sup>4</sup>, U. Zeitler<sup>4</sup>, Y. Tokunaga<sup>5,6</sup>, Y. Taguchi<sup>5</sup>, and Y. Tokura<sup>5,7</sup>

<sup>1</sup>*Materials Science and Technology Division, Oak Ridge National Laboratory, Oak Ridge, Tennessee 37831, USA*

<sup>2</sup>*Department of Physics, Budapest University of Technology and Economics and MTA-BME*

*Lendület Magneto-optical Spectroscopy Research Group, 1111 Budapest, Hungary*

<sup>3</sup>*National Institute of Chemical Physics and Biophysics, Akadeemia tee 23, 12618 Tallinn, Estonia*

<sup>4</sup>*High Field Magnet Laboratory (HFML-EMFL), Radboud University Nijmegen,*

*Toernooiveld 7, 6525 ED Nijmegen, The Netherlands*

<sup>5</sup>*RIKEN Center for Emergent Matter Science (CEMS), Wako, Saitama 351-0198, Japan*

<sup>6</sup>*Department of Advanced Materials Science, University of Tokyo, Kashiwa 277-8561, Japan and*

<sup>7</sup>*Department of Applied Physics, University of Tokyo, Hongo, Tokyo 113-8656, Japan*

(Dated: March 3, 2019)

Competing exchange interactions can produce complex magnetic states together with spin-induced electric polarizations. With competing interactions on alternating triangular and kagome layers, the swedenborgite  $\text{CaBaCo}_4\text{O}_7$  may have one of the largest measured spin-induced polarizations of  $\sim 1700$  nC/cm<sup>2</sup> below its ferrimagnetic transition temperature at 70 K. Powder neutron-diffraction data, magnetization measurements, and spin-wave resonance frequencies in the THz range reveal that the complex spin order of multiferroic  $\text{CaBaCo}_4\text{O}_7$  can be described as a triangular array of  $c$ -axis chains ferrimagnetically coupled to each other in the  $ab$  plane. Magnetostriction on bonds that couple those chains produces the large spin-induced polarization of  $\text{CaBaCo}_4\text{O}_7$ .

PACS numbers: 75.25.-j, 75.30.Ds, 75.50.Ee, 78.30.-j

Competing exchange interactions produce complex magnetic states with a wide range of interesting behavior found in spin glass [1], spin ice [2], and magnetic skyrmions [3]. In multiferroic materials, complex spin states can exhibit a spin-induced electric polarization  $\mathbf{P}$  due to either the spin current,  $p$ - $d$  orbital hybridization, or magnetostriction [4,5]. Because the coupling between the electrical and magnetic properties in multiferroic materials is both scientifically and technologically important, the effects of competing exchange interactions have been investigated in a wide range of multiferroic materials such as  $\text{RMnO}_3$  [6],  $\text{CoCrO}_4$  [7],  $\text{CuCrO}_2$  [8],  $\text{CuFeO}_2$  [9], and  $\text{MnWO}_4$  [10]. While the first four materials [6–9] are geometrically frustrated due to competing interactions on a triangular lattice,  $\text{MnWO}_4$  [10] exhibits long-range competing interactions [11] on a highly-distorted monoclinic lattice.

Compounds in the “114” swedenborgite family [12]  $\text{RBaM}_4\text{O}_7$  ( $M = \text{Co}$  or  $\text{Fe}$ ) contain alternating triangular and kagome layers, both of which are geometrically frustrated when undistorted. The “114” cobaltites [13–

15] were initially studied to find charge ordering among the  $\text{Co}^{2+}$  and  $\text{Co}^{3+}$  ions. An important member of this family,  $\text{YBaCo}_4\text{O}_7$  exhibits antiferromagnetic ordering [16,17] below 110 K and diffuse scattering [13,14] indicative of spin disorder below 60 K. The magnetic state between 110 K and 60 K is stabilized by a structural transition [18] that relieves the geometric frustration. Both structural and magnetic transitions are quite sensitive to excess oxygen and no magnetic order [19,20] appears in  $\text{YBaCo}_4\text{O}_{7+\delta}$  for  $\delta \geq 0.12$ . Another family member,  $\text{YbBaCo}_4\text{O}_7$  undergoes a structural transition at 175 K that stabilizes an antiferromagnetic state below 80 K [21].

A particularly interesting “114” cobaltite,  $\text{CaBaCo}_4\text{O}_7$  undergoes an orthorhombic distortion [22,23] that relieves the geometric magnetic frustration on both the kagome and triangular layers sketched in Fig. 1 above the magnetic transition temperature  $T_c = 70$  K. Below  $T_c$ ,  $\text{CaBaCo}_4\text{O}_7$  develops a very large spin-induced polarization  $\sim 1700$  nC/cm<sup>2</sup> [24], second only to the conjectured [25] spin-induced polarization  $\sim 3000$  nC/cm<sup>2</sup> of  $\text{BiFeO}_3$ . Also unusual,  $\text{CaBaCo}_4\text{O}_7$  generates a substantial ferrimagnetic moment of about  $0.9 \mu_B$  per formula unit (f.u.) [26], which could allow magnetic control of the electric polarization. Although its ferroelectric transition is inaccessible and its permanent electric polarization is not switchable [27], applications of  $\text{CaBaCo}_4\text{O}_7$  might utilize the large spin-induced polarization produced by a magnetic field just below  $T_c$  [24].

This Letter solves for the magnetic properties of  $\text{CaBaCo}_4\text{O}_7$  based on a Heisenberg model with 12 nearest neighbor interactions and associated anisotropies. The magnetic state of  $\text{CaBaCo}_4\text{O}_7$  can be described as a triangular array of ferrimagnetically aligned  $c$ -axis chains with net moment along  $\mathbf{b}$ . Competing interactions within

\*Copyright notice: This manuscript has been authored by UT-Battelle, LLC under Contract No. DE-AC05-00OR22725 with the U.S. Department of Energy. The United States Government retains and the publisher, by accepting the article for publication, acknowledges that the United States Government retains a non-exclusive, paid-up, irrevocable, world-wide license to publish or reproduce the published form of this manuscript, or allow others to do so, for United States Government purposes. The Department of Energy will provide public access to these results of federally sponsored research in accordance with the DOE Public Access Plan (<http://energy.gov/downloads/doe-public-access-plan>).

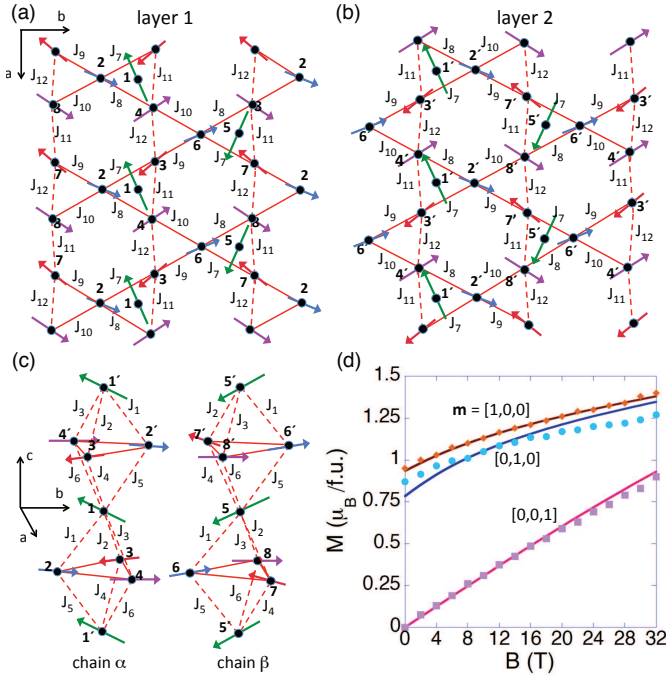


FIG. 1: (Color online) (a) and (b) The predicted spin configuration for layers 1 and 2 in zero field. (c) A sideways view showing  $c$ -axis chains  $\alpha$  and  $\beta$ . (d) The measured (circles and squares) and predicted (solid curves) magnetizations for field along  $[1, 0, 0]$ ,  $[0, 1, 0]$ , or  $[0, 0, 1]$ .

each chain produce a non-collinear spin state. The strong spin-induced electric polarization below  $T_c$  is caused by the electric-field dependence of the interactions that couple those chains due to the displacement of the surrounding oxygen atoms in an electric field.

Each magnetic unit cell of  $\text{CaBaCo}_4\text{O}_7$  contains 16 Co ions on two kagome and two triangular layers with orthorhombic lattice constants  $a = 6.3 \text{ \AA}$ ,  $b = 11.0 \text{ \AA}$ , and  $c = 10.2 \text{ \AA}$ . Four crystallographically distinct Co ions have three different valences [22,28]. The triangular layers contain mixed-valent  $\text{Co}^{3+}/\text{Co}^{2+}\underline{L}$  ( $\underline{L}$  is a ligand hole) spins 1, 5, 9, and 13 with moments  $M_1 = 2.9 \mu_B$ . The kagome layers contain  $\text{Co}^{2+}$  spins 2, 3, 6, 7, 10, 11, 14, and 15 with moments  $M_2 = M_3 = 2 \mu_B$  and mixed-valent  $\text{Co}^{3+}/\text{Co}^{2+}\underline{L}$  spins 4, 8, 12, and 16 with  $M_4 = 2.4 \mu_B$ . Because adjacent kagome or triangular layers are related by symmetry,  $\mathbf{S}_{i'} = \mathbf{S}_{i+8}$  on layer two is identical to  $\mathbf{S}_i$  on layer one. With  $\mathbf{S}_i = S_i(\cos \phi_i, \sin \phi_i, 0)$  constrained to the  $ab$  plane, the ferrimagnetic moment lies along  $\mathbf{b}$  if  $\phi_{i+4} = \pi - \phi_i$  ( $i = 1, \dots, 4$ ).

The 12 different nearest-neighbor exchange couplings  $J_i$  are drawn in Figs. 1(a-c). Six of these ( $J_1$  through  $J_6$ ) couple the kagome and triangular layers as shown in Fig. 1(c); the other six ( $J_7$  through  $J_{12}$ ) couple the spins within a kagome layer as shown in Figs. 1(a) and (b). The dominance of nearest-neighbor exchange over next-nearest neighbor exchange [27] justifies setting the exchange interactions between spins on the triangular layers

to zero. Our model also includes easy-plane anisotropies  $D$ , easy-axis anisotropies  $C$  within both kagome and triangular layers, and hexagonal anisotropy  $A$  on the triangular layers.

With magnetic field  $\mathbf{B}$  along  $\mathbf{m}$ , the Hamiltonian is

$$\begin{aligned} \mathcal{H} = & - \sum_{\langle i,j \rangle} J_{ij} \mathbf{S}_i \cdot \mathbf{S}_j + D^{\text{tri}} \sum_{i,\text{tri}} S_{ic}^2 + D^{\text{kag}} \sum_{i,\text{kag}} S_{ic}^2 \\ & - C^{\text{kag}} \sum_{i,\text{kag}} (\mathbf{o}_i \cdot \mathbf{S}_i)^2 - C^{\text{tri}} \sum_{i,\text{tri}} (\mathbf{n}_i \cdot \mathbf{S}_i)^2 \\ & - A^{\text{tri}} S_1^6 \sum_{i,\text{tri}} \cos 6\phi_i - 2\mu_B B \sum_i \mathbf{m} \cdot \mathbf{S}_i, \end{aligned} \quad (1)$$

where  $\mathbf{S}_i$  is a spin  $S$  operator on site  $i$ . The easy-axis anisotropy terms proportional to  $C^{\text{kag}}$  and  $C^{\text{tri}}$  involve unit vectors  $\mathbf{o}_i$  along the “bowtie” directions  $\phi_i = \pi/2$  (spins 2 and 6),  $5\pi/6$  (spins 3 and 8) and  $7\pi/6$  (spins 4 and 7) for the kagome layers and  $\mathbf{n}_i$  along the  $\phi_i = \pi/6$  (spin 1) and  $-\pi/6$  (spin 5) directions for the triangular layers. Note that all anisotropy terms may act to constrain the spins to the  $ab$  plane.

The spin amplitudes  $S_n$  are fixed at their observed values  $M_n/2\mu_B$  after performing a  $1/S$  expansion about the classical limit. Static properties are obtained by minimizing the classical energy  $\langle \mathcal{H} \rangle$  (the zeroth-order term in this expansion) with respect to the 16 spin angles. The eigenvalues and eigenvectors of a  $32 \times 32$  equations-of-motion matrix [29] produced by the second-order term give the optical mode frequencies and their absorptions, respectively.

Perhaps due to excess or deficient oxygen [30] or different domain populations (see below), previous magnetization measurements [22,26,31–33] on  $\text{CaBaCo}_4\text{O}_7$  are rather scattered. Our fits are based on new magnetization measurements performed at 4 K on hexagonally-twinned crystals with a common  $\mathbf{c} = \mathbf{z} = [0, 0, 1]$  axis. In domain I,  $\mathbf{a}$  lies along the laboratory direction  $\mathbf{x} = [1, 0, 0]$  and  $\mathbf{b}$  lies along  $\mathbf{y} = [0, 1, 0]$ ; in domain II,  $\mathbf{a} = [-1/2, \sqrt{3}/2, 0]$  and  $\mathbf{b} = [-\sqrt{3}/2, -1/2, 0]$ ; and in domain III,  $\mathbf{a} = [-1/2, -\sqrt{3}/2, 0]$  and  $\mathbf{b} = [\sqrt{3}/2, -1/2, 0]$ . If  $p_n$  are the domain populations, then the magnetizations  $M_x$  and  $M_y$  measured with fields along  $\mathbf{x}$  and  $\mathbf{y}$  only depend on  $p_1$  and  $p_2 + p_3 = 1 - p_1$ . Of course,  $M_z$  measured with field along  $\mathbf{z}$  is independent of  $p_n$ . Fig. 1(d) indicates that all three magnetizations increase monotonically up to at least 32 T.

Previous optical measurements [34] at the ordering wavevector  $\mathbf{Q}$  found two conventional spin-wave modes that couple to the ground state through the magnetization operator  $\mathbf{M} = 2\mu_B \sum_i \mathbf{S}_i$ . These magnetic-resonance (MR) modes are degenerate in zero field with a frequency of 1.07 THz and split almost linearly with increasing field along  $\mathbf{y}$ , as shown in Fig. 2. For  $\mathbf{m} = \mathbf{y}$ , the MR modes are excited in two geometries: (i) with THz fields  $\mathbf{E}_\omega \parallel \mathbf{x}$  and  $\mathbf{B}_\omega \parallel \mathbf{z}$  and (ii) with  $\mathbf{E}_\omega \parallel \mathbf{z}$  and  $\mathbf{B}_\omega \parallel \mathbf{x}$ . Those measurements also found an electromagnon (EM) that couples to the ground state through the polarization

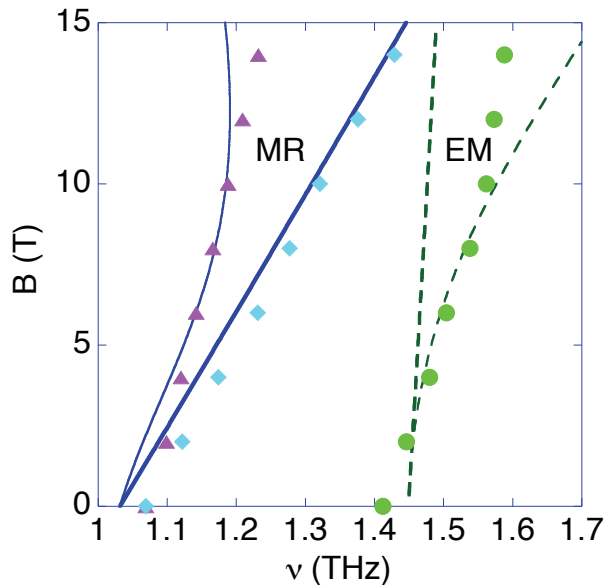


FIG. 2: (Color online) The predicted MR (solid) and EM (dashed) modes for domain I (thick) and domains II and III (thin). Measured modes are indicated by solid points.

operator  $\mathbf{P}$ . The EM with zero-field frequency 1.41 THz is only excited in geometry *ii*.

Because the exchange couplings already break every degeneracy in the unit cell, the 16 predicted modes for a single domain are non-degenerate. Therefore, the split MR modes must come from different domains. This was verified by measuring [35] the MR mode frequencies as a function of the rotation angle  $\theta$  for field  $\mathbf{B} = B(\cos\theta, \sin\theta, 0) = B(\mathbf{x}\cos\theta + \mathbf{y}\sin\theta)$  in the laboratory reference frame. As shown in Fig. 3 for 12 and 15 T, each hexagonal domain contributes one MR branch with a period of  $\pi$ .

With field  $\mathbf{B}_{\text{loc}} = B(\cos\psi, \sin\psi, 0) = B(\mathbf{a}\cos\psi + \mathbf{b}\sin\psi)$  in the domain reference frame, the upper MR mode in Fig. 2 corresponds to the  $\psi = \pi/2$  mode for domain I while the lower MR mode corresponds to the degenerate  $\psi = \pm\pi/6$  modes for domains II and III. Previously measured MR frequencies plotted in Fig. 2 at 12 T correspond to the diamond and triangular points in Fig. 3(b) at  $\theta = \pi/2$ . Cusps in the MR curves for each domain at  $\psi = 0$  and  $\pi$  are caused by flipping the  $b$  component of the magnetization (see inset to Fig. 3(b)).

Fits for the coupling parameters utilize the field dependence of  $\mathbf{M}$ , the zero-field powder neutron-diffraction data [22], the field dependence of the MR and EM modes at  $\theta = \pi/2$  [34], and the MR mode frequencies at  $\theta = 0$  and  $\pi/3$  for 7, 12 and 15 T. The resulting exchange and anisotropy constants are provided in Table I and the corresponding zero-field spin state is plotted in Figs. 1(a-c). In contrast to the previously proposed [22] spin state with zig-zag chains in the  $ab$  plane containing spins 2, 3, 6, and 7, our spin state can be better described as an array of  $c$ -axis chains or connected bitetrahedra [16,36] contain-

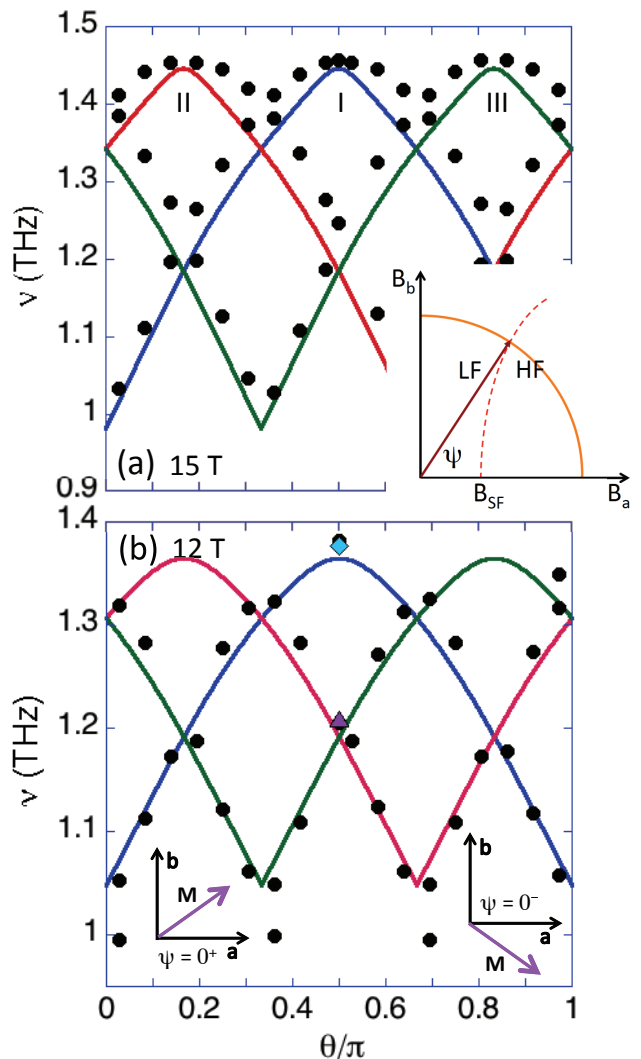


FIG. 3: (Color online) The measured (solid circles) and predicted (blue, red, and green curves for domains I, II, and III, respectively) angular dependence of the MR mode frequencies for 12 and 15 T. The inset to (a) sketches the angular dependence of  $\mathbf{B}_{\text{SF}}$  (dashed curve), which separates low-field (LF) and high-field (HF) states. The inset to (b) shows the net magnetization of any domain for angles  $\psi$  on either side of 0. Flips of the  $b$ -axis spin at  $\psi = 0$  and  $\pi$  produce the cusps in the mode frequencies.

ing spins  $\{1, 2, 3, 4\}$  (chain  $\alpha$ ) or  $\{5, 6, 7, 8\}$  (chain  $\beta$ ) as sketched in Fig. 1(c). Chains are coupled by exchanges  $J_9$ ,  $J_{10}$ , and  $J_{12}$  in the  $ab$  plane. Given other conditions, our fit chooses the spin state that matches the powder-diffraction data [22] as closely as possible [37]. At zero field, the predicted spin state has angles  $\phi_1 = -0.83\pi$ ,  $\phi_2 = 0.39\pi$ ,  $\phi_3 = -0.23\pi$ , and  $\phi_4 = 0.62\pi$ .

What explains the wide range of  $J_i$  values? An orthorhombic distortion [22,23] with  $b/(a\sqrt{3}) - 1 \rightarrow 0.018$  as  $T \rightarrow 0$  breaks the hexagonal symmetry of the  $ab$  plane and explains the difference between the pairs  $\{J_1, J_2\}$ ,  $\{J_8, J_{11}\}$ , and  $\{J_{10}, J_{12}\}$ . The difference between cou-

TABLE I: Exchange and anisotropy parameters in meV.

	$p_1$	$J_1 = J_5$	$J_2 = J_4$	$J_3 = J_6$	$J_7$	$J_8$	$J_9$	$J_{10}$	$J_{11} = J_{12}$	$D^{\text{kag}}$	$D^{\text{tri}}$	$C^{\text{kag}}$	$C^{\text{tri}}$	$S_1^4 A^{\text{tri}}$
	0.18	-92.7	-10.6	41.5	-29.5	181	6.6	94.7	-5.6	-0.52	-1.38	3.52	0.92	0.03
error	$\pm 0.08$	$\pm 4.0$	$\pm 0.5$	$\pm 0.9$	$\pm 2.1$	$\pm 9$	$\pm 0.5$	$\pm 6.3$	$\pm 0.4$	$\pm 0.06$	$\pm 0.03$	$\pm 0.20$	$\pm 0.07$	$\pm 0.01$

plings like  $\{J_7, J_8\}$  is caused by charge ordering: whereas  $J_7$  couples moments 2 and 3 with  $M_2 = M_3$ ,  $J_8$  couples moments 2 and 4 with  $M_2 \neq M_4$ . Charge ordering also explains the difference between the pairs  $\{J_2, J_3\}$  and  $\{J_9, J_{10}\}$ . Although not demanded by symmetry, we set  $J_1 = J_5$ ,  $J_2 = J_4$ ,  $J_3 = J_6$ , and  $J_{11} = J_{12}$  because the spin state and excitations at  $\mathbf{Q}$  only depend on their averages [38].

Our results indicate that the exchange coupling  $J_8 \approx 181$  meV between moments 2 ( $\text{Co}^{2+}$ ) and 4 ( $\text{Co}^{3+}/\text{Co}^{2+}\underline{\text{L}}$ ) is strongly ferromagnetic and larger in magnitude even than the 155 meV antiferromagnetic coupling found in the cuprate  $\text{Nd}_2\text{CuO}_4$  [39]. The strength of this coupling might be explained by the double-exchange mediated hopping of ligand holes  $\underline{\text{L}}$  [19] from site 4 to 2.

Except for  $J_{10}$ , the five largest exchange couplings  $J_1 = J_5 \approx -93$  meV,  $J_3 = J_6 \approx 42$  meV, and  $J_8 \approx 181$  meV lie within connected bitetrahedral,  $c$ -axis chains. Inside each chain, competing interactions between spins 1, 2, and 4 produce a non-collinear spin state.

Although lying on a triangular lattice, chains  $\alpha$  and  $\beta$  are magnetically ordered with moments  $\mathbf{M}^{\text{ch}} = (\pm 1.20, 1.32, 0)\mu_{\text{B}}/\text{f.u.}$ . Chains  $\alpha$  and  $\beta$  are primarily coupled by the strongly ferromagnetic interaction  $J_{10} \approx 95$  meV between nearly parallel spins  $\{4, 6\}$  ( $\phi_4 = 0.62\pi$ ,  $\phi_6 = 0.61\pi$ ) and  $\{2, 8\}$  ( $\phi_2 = 0.39\pi$ ,  $\phi_8 = 0.38\pi$ ). Above  $T_c = 70$  K, the short-range order within each chain may be responsible for the large, negative Curie-Weiss temperature  $\Theta_{\text{CW}} \approx -1720$  [26] or  $-890$  K [31], the larger than expected Curie constant [26], and the susceptibility anomaly [31] at 360 K suggestive of short-range magnetic order far above  $T_c$ .

Comparison between the theoretical and experimental results for the magnetization in Fig. 1(d) suggests that roughly 20% of the sample is in domain I. Different domain populations or even orthorhombic twinning in other samples may explain the discrepancies between the reported magnetization measurements [22,26,31–33].

Easy-axis anisotropies  $A$  and  $C$  favor ferrimagnetic alignment along  $\mathbf{b}$  rather than  $\mathbf{a}$ . The spin-flop (SF) field required to flip the spins towards the  $\mathbf{a}$  direction must increase as the field along  $\mathbf{b}$  increases [40]. As shown in the inset to Fig. 3(a),  $B_{\text{SF}}(\psi)$  then increases with  $\psi$ . If  $B_{\text{SF}}(\psi = 0) < 15$  T, then the MR spectrum for 15 T would show a discontinuity at the transition from a low-field (LF) to a high-field (HF) state below some critical value of  $\psi$ . Since the MR mode frequencies in Fig. 3(a) do not exhibit a discontinuity as a function of  $\psi$ , we conclude that  $B_{\text{SF}}(\psi = 0)$  exceeds 15 T and probably, based on the smooth dependence of the magnetizations on field, exceeds 32 T as well. The apparent small size

of  $B_{\text{SF}}$  [24,41] must reflect the net magnetization of all three domains.

Predicted modes below 5 THz are plotted in Fig. 2. The Goldstone modes for all three domains are lifted by in-plane anisotropies to become the MR modes with zero-field frequencies of 1.07 THz. As remarked earlier, the lower MR mode comes from domains II and III while the upper MR mode comes from domain I. Below 3.5 THz, one EM mode is produced in domain I and another in domains II and III. The degenerate EM modes from domains II and III dominate the optical absorption. The predicted field dependence of the upper MR mode is quite close to the observed dependence. But the predicted curvatures of the lower MR mode and the EM mode, both from domains II and III, is not observed.

Note that the electric-field dependence of the easy-plane anisotropy  $D$  cannot explain the spontaneous, spin-induced polarization along  $\mathbf{c}$  that appears below  $T_c$  because the expectation value of  $P_i = \kappa S_{ic}^2$  with  $\kappa = -\partial D/\partial E_c$  would vanish in zero magnetic field when all the spins are in the  $ab$  plane. Easy-axis anisotropy  $A$  or  $C$  in the  $ab$  plane could produce a spin-induced electric polarization perpendicular to  $\mathbf{c}$ . But the EM mode would then become observable for a THz electric field in the  $ab$  plane, contrary to measurements.

As conjectured previously [24], the spin-induced polarization in  $\text{CaBaCo}_4\text{O}_7$  must be generated by the dependence of the exchange interactions  $J_{ij}$  on an electric field, called magnetostriction. Coupling constant  $\lambda_{ij}$  for bond  $\{i, j\}$  is associated with the spin-induced polarization [42] per site of  $P_c^{ij} = \lambda_{ij} \mathbf{S}_i \cdot \mathbf{S}_j/4$  (accounting for the four equivalent bonds per unit cell) with  $\lambda_{ij} = \partial J_{ij}/\partial E_c$ . The MR matrix element  $\langle n|M_a|0\rangle$  mixes with the EM matrix element  $\langle n|P_c^{ij}|0\rangle$  for domains II and III but not for domain I. Therefore, our model can explain the strong asymmetry [43]  $\sim \text{Re}\{\langle n|\mathbf{M} \cdot \mathbf{B}_\omega|0\rangle\langle 0|\mathbf{P} \cdot \mathbf{E}_\omega|n\rangle\}$  in the absorption of counter-propagating light waves [34] for the lower observed MR mode in geometry  $ii$  with  $\mathbf{E}_\omega \parallel \mathbf{c}$ . But it cannot explain the observed asymmetry of this mode in geometry  $i$  with  $\mathbf{E}_\omega \perp \mathbf{c}$  if only  $\langle 0|P_c|n\rangle$  is significant.

The bonds responsible for the spin-induced polarization can be enumerated based on the observation that the EM mode has an absorption about 7.5 times that of the MR mode in zero field, rising to about 35 times the upper MR mode at 10 T. At both 0 and 10 T, the only sets of bonds that generate spin-induced polarizations of the right magnitude are  $\{2, 7\}$  and  $\{3, 4\}$ , both coupling adjacent  $c$ -axis chains [37] through pairs of spins that are almost anti-parallel. From the relative absorptions at 0 T, we estimate that  $\langle P_c^{27}\rangle \approx 2340$  nC/cm<sup>2</sup> and  $\langle P_c^{34}\rangle \approx 2050$  nC/cm<sup>2</sup>. These results are roughly

consistent with the recently observed [24] polarization of  $1700 \text{ nC/cm}^2$  but significantly higher than the density-functional theory result [27]  $\langle P_c \rangle \approx 460 \text{ nC/cm}^2$ . Note that other measurements indicate that  $\langle P_c \rangle$  ranges from  $320 \text{ nC/cm}^2$  [32] to  $900 \text{ nC/cm}^2$  [44]. The spin-induced polarization should remain fairly constant with applied magnetic field, decreasing by about 1% for a 10 T field along  $\mathbf{b}$ .

We have presented a nearly complete solution for the magnetization, spin state, and mode frequencies of the swedenborgite  $\text{CaBaCo}_4\text{O}_7$ . An orthorhombic distortion above  $T_c$  partially relieves the geometric frustration on the kagome and triangular layers and allows ferrimagnetism and ferroelectricity to coexist below  $T_c$ . Although occupying a triangular lattice, the  $c$ -axis chains are ferrimagnetically ordered in the  $ab$  plane. Competing interactions within each chain produce non-collinear spin states. Sets of bonds coupling those chains are responsible for the large spin-induced polarization of  $\text{CaBaCo}_4\text{O}_7$ .

Despite its fixed permanent electric polarization, this swedenborgite may have important technological applications utilizing the large changes [24] in the spin-induced polarization when a modest magnetic field  $< 1 \text{ T}$  is applied along  $\mathbf{b}$  just below  $T_c$ . A big jump in the polarization should also be produced just below  $T_c$  by rotating a fixed magnetic field about the  $c$  axis. Above all, our work illuminates a pathway to develop other functional materials with sizeable magnetic moments and electrical polarizations.

Research sponsored by the U.S. Department of Energy, Office of Science, Basic Energy Sciences, Materials Sciences and Engineering Division (RF), by the Hungarian Research Funds OTKA K 108918, OTKA PD 111756, and Bolyai 00565/14/11 (SB, VK, and IK), and by the institutional research funding IUT23-3 of the Estonian Ministry of Education and Research and the European Regional Development Fund project TK134 (TR and UN).

- 
- <sup>1</sup> K. Binder and A.P. Young, *Rev. Mod. Phys.* **58**, 801 (1986).
- <sup>2</sup> M.J. Harris, S.T. Bramwell, D.F. McMorrow, T. Zeiske, and K.W. Godfrey, *Phys. Rev. Lett.* **79**, 2554 (1997).
- <sup>3</sup> S. Mühlbauer, B. Binz, F. Jonietz, C. Pfleiderer, A. Rosch, A. Neubauer, R. Georgii, and P. Böni, *Science* **323**, 915 (2011).
- <sup>4</sup> D.I. Khomskii, *J. Magn. Magn. Mater.* **306**, 1 (2006).
- <sup>5</sup> S.-W. Cheong and M. Mostovoy, *Nat. Mat.* **6**, 13 (2007).
- <sup>6</sup> A.B. Sushkov, R.V. Aguilar, S. Park, S.-W. Cheong, and H.D. Drew, *Phys. Rev. Lett.* **98**, 027202 (2007).
- <sup>7</sup> Y. Yamasaki, S. Miyasaka, Y. Kaneko, J.-P. He, T. Arima, and Y. Tokura, *Phys. Rev. Lett.* **96**, 207204 (2006).
- <sup>8</sup> M. Soda, K. Kimura, T. Kimura, and K. Hirota, *Phys. Rev. B* **81**, 100406 (2010).
- <sup>9</sup> S. Seki, N. Kida, S. Kumakura, R. Shimano, and Y. Tokura, *Phys. Rev. Lett.* **105**, 097207 (2010).
- <sup>10</sup> K. Taniguchi, N. Abe, S. Ohtani, and T. Arima, *Phys. Rev. Lett.* **102**, 147201 (2009).
- <sup>11</sup> F. Ye, R.S. Fishman, J.A. Fernandez-Baca, A.A. Podlesnyak, G. Ehlers, H.A. Mook, Y.-Q. Wang, B. Lorenz, and C.W. Chu, *Phys. Rev. B* **83**, 140401 (2011).
- <sup>12</sup> B. Raveau, V. Caignaert, V. Pralong, and A. Maignan, *Z. Anorg. Allg. Chem.* **635**, 1869 (2012).
- <sup>13</sup> M. Valldor and M. Andersson, *Sol. St. Sci.* **4**, 923 (2002); M. Valldor, *Sol. St. Sci.* **6**, 251 (2004).
- <sup>14</sup> E.V. Tsipis, D.D. Khalyavin, S.V. Shiryayev, K.S. Redkina, and P. Núñez, *Mat. Chem. Phys.* **92**, 33 (2005); E.V. Tsipis, V.V. Kharton, J.R. Frade, and P. Núñez, *J. Sol. St. Electrochem.* **9**, 547 (2005).
- <sup>15</sup> G.L. Bychkov, S.N. Barilo, S.V. Shiryayev, D.V. Sheptyakov, S.N. Ustinovich, A. Podlesnyak, M. Baran, R. Szymczak, and A. Furrer, *J. Cryst. Growth* **275**, e813 (2005).
- <sup>16</sup> L.C. Chapon, P.G. Radaelli, H. Zheng, and J.F. Mitchell, *Phys. Rev. B* **74**, 172401 (2006).
- <sup>17</sup> D.D. Khalyavin, P. Manuel, B. Ouladdiaf, A. Huq, P.W. Stephens, H. Zheng, J.F. Mitchell, and L.C. Chapon, *Phys. Rev. B* **83**, 094412 (2011).
- <sup>18</sup> A.K. Bera, S.M. Yusuf, and S. Banerjee, *Sol. St. Sci.* **16**, 57 (2013).
- <sup>19</sup> A. Maignan, V. Caignaert, D. Pelloquin, S. Hébert, V. Pralong, J. Hejtmanek, and D. Khomskii, *Phys. Rev. B* **74**, 165110 (2006).
- <sup>20</sup> S. Avci, O. Chmaissem, H. Zheng, A. Huq, P. Manuel, and J.F. Mitchell, *Chem. Mat.* **25**, 4188 (2013).
- <sup>21</sup> A. Huq, J.F. Mitchell, H. Zheng, L.C. Chapon, P.G. Radaelli, K.S. Knight, and P.W. Stephens, *J. Sol. St. Chem.* **179**, 1136 (2006).
- <sup>22</sup> V. Caignaert, V. Pralong, V. Hardy, C. Ritter, and B. Raveau, *Phys. Rev. B* **81**, 094417 (2010).
- <sup>23</sup> S.N. Panja, J. Kumar, S. Dengre, and S. Nair, *J. Phys.: Cond. Mat.* **16**, 9209 (2016).
- <sup>24</sup> V. Caignaert, A. Maignan, K. Singh, Ch. Simon, V. Pralong, B. Raveau, J.F. Mitchell, H. Zheng, A. Huq, and L.C. Chapon, *Phys. Rev. B* **88**, 174403 (2013).
- <sup>25</sup> J.-H. Lee and R.S. Fishman, *Phys. Rev. Lett.* **115**, 207203 (2015).
- <sup>26</sup> V. Caignaert, V. Pralong, A. Maignan, and B. Raveau, *Sol. St. Comm.* **149**, 453 (2009).
- <sup>27</sup> R.D. Johnson, K. Cao, F. Giustino, and P.G. Radaelli, *Phys. Rev. B* **90**, 045192 (2014).
- <sup>28</sup> S. Chatterjee and T. Saha-Dasgupta, *Phys. Rev. B* **84**, 085116 (2011).
- <sup>29</sup> R.S. Fishman, J.T. Haraldsen, N. Furukawa, and S. Miyahara, *Phys. Rev. B* **87**, 134416 (2013).
- <sup>30</sup> Md. M. Seikh, V. Caignaert, V. Pralong, and B. Raveau, *J. Phys. Chem. Sol.* **75**, 79 (2014).
- <sup>31</sup> Z. Qu, L. Ling, L. Zhang, and Y. Zhang, *Sol. St. Comm.* **151**, 917 (2011).
- <sup>32</sup> H. Iwamoto, M. Ehara, M. Akaki, and H. Kuwahara, *J. Phys.: Conf. Ser.* **400**, 032031 (2012).
- <sup>33</sup> Md. M. Seikh, T. Sarkar, V. Pralong, V. Caignaert, and B. Raveau, *Phys. Rev. B* **86**, 184403 (2012).
- <sup>34</sup> S. Bordács, V. Kocsis, Y. Tokunaga, U. Nagel, T. Rődm, Y. Takahashi, Y. Taguchi, and Y. Tokura, *Phys. Rev. B* **92**, 214441 (2015).
- <sup>35</sup> The THz spectra of  $\text{CaBaCo}_4\text{O}_7$  were measured at 2.5 K

with linear light polarization using Fourier-transform spectroscopy [34]. The reference spectrum was taken in zero field.

<sup>36</sup> M. Valldor, *J. Phys.: Cond. Mat.* **16**, 9209 (2004).

<sup>37</sup> See supplementary material.

<sup>38</sup> Spin excitations away from  $\mathbf{q} = \mathbf{Q}$  depend separately on these exchange constants. The stability of the coplanar ground state requires that each pair of exchange constants be sufficiently close to one another.

<sup>39</sup> P. Bourges, H. Casalta, A.S. Ivanov, and D. Petitgrand, *Phys. Rev. Lett.* **79**, 4906 (1997).

<sup>40</sup> While the coplanar LF spin state has a lower energy than the HF state below 32 T, it becomes locally unstable to a buckled state with spins canted out of the  $ab$  plane between 16 and 32 T for field along  $\mathbf{a}$ . Based on the smooth dependence of the magnetizations on field, the transition from the coplanar to the buckled state must be second order.

<sup>41</sup> V. Pralong, V. Caignert, T. Sarkar, O.I. Lebedev, V. Duf-

fort, and B. Raveau, *J. Sol. St. Chem.* **184**, 2588 (2011).

<sup>42</sup> Based on the symmetry of adjacent layers, it is easy to show that the polarization operator  $\mathbf{P}^{12}$  associated with bond  $\{1, 2\}$  has components

$$P_a^{12} \propto C_{12} - C_{56} - C_{1'2'} + C_{5'6'},$$

$$P_b^{12} \propto C_{12} + C_{56} - C_{1'2'} - C_{5'6'},$$

$$P_c^{12} \propto C_{12} + C_{56} + C_{1'2'} + C_{5'6'},$$

where  $C_{ij} = \mathbf{S}_i \cdot \mathbf{S}_j$ . Similar relations hold for other bonds. Only the  $c$  component  $P_c^{ij}$  can produce a static polarization but all three components may contribute to the off-diagonal polarization matrix elements  $\langle 0 | P_\alpha^{ij} | n \rangle$  ( $n \neq 0$ ).

<sup>43</sup> S. Miyahara and N. Furukawa, *J. Phys. Soc. Japan* **80**, 073708 (2011).

<sup>44</sup> V. Koscis, S. Bordács, and I. Kézsmárki, (unpublished).